

# Thermal analysis and cooling structure design of the primary collimator in CSNS/RCS

ZOU Yi-Qing()<sup>1,2,1)</sup> WANG Na()<sup>1</sup> KANG Ling()<sup>1</sup>  
 QU Hua-Min()<sup>1</sup> HE Zhe-Xi()<sup>1,2</sup> YU Jie-Bing()<sup>1</sup>

<sup>1</sup> Institute of High Energy Physics, Chinese Academy of Sciences, Beijing 100049, China

<sup>2</sup> Graduate University of Chinese Academy of Sciences, Beijing 100049, China

**Abstract:** The rapid cycling synchrotron (RCS) of the China Spallation Neutron Source (CSNS) is a high intensity proton ring with beam power of 100 kW. In order to control the residual activation to meet the requirements of hands-on maintenance, a two-stage collimation system has been designed for the RCS. The collimation system consists of one primary collimator made of thin metal to scatter the beam and four secondary collimators as absorbers. Thermal analysis is an important aspect in evaluating the reliability of the collimation system. The calculation of the temperature distribution and thermal stress of the primary collimator with different materials is carried out by using ANSYS code. In order to control the temperature rise and thermal stress of the primary collimator to a reasonable level, an air cooling structure is intended to be used. The mechanical design of the cooling structure is presented, and the cooling efficiency with different chin numbers and wind velocity is also analyzed. Finally, the fatigue lifetime of the collimator under thermal shocks is estimated.

**Key words:** primary collimator, cooling structure, thermal analysis, fatigue lifetime

**PACS:** 29.27.Eg, 44.05.+e, 44.10.+i **DOI:** 10.1088/1674-1137/37/5/057004

## 1 Introduction

In high intensity proton rings, beam induced activation is a primary concern during the design of the accelerators. To achieve hands-on maintenance, the beam loss should be well controlled below 1 W/m, which is hard to achieve during the design and construction of an actual machine. A beam collimation system is often used to concentrate the beam loss in a restricted area to reduce beam loss deposition in other areas around the ring [1].

The CSNS will provide beam pulses of  $1.56 \times 10^{13}$  particles with repetition rate of 25 Hz. The RCS is designed to accelerate the proton beam from 80 MeV to 1.6 GeV [2]. A two-stage collimation system will be used for the transverse beam collimation in the RCS. Halo particles with large amplitude will first hit the primary collimator. After interaction, the particles will be scattered by the primary collimator without being absorbed. Then, after some certain distance, the particles will finally be absorbed by the secondary collimators downstream from the primary one [3, 4].

The primary collimator consists of four scrapers, which are set either horizontally or vertically as shown in Fig. 1. Each scraper has a dimension of 150 mm×30 mm ( $W \times H$ ) in the transverse plane. Movable collimators with

air cooling are chosen for the transverse beam collimation in CSNS. This piece is brazed to an air-cooled copper block. Fig. 4 shows the detail of the scraper mechanism. The scraper slice, bellow, slide and cooling fin can be seen.

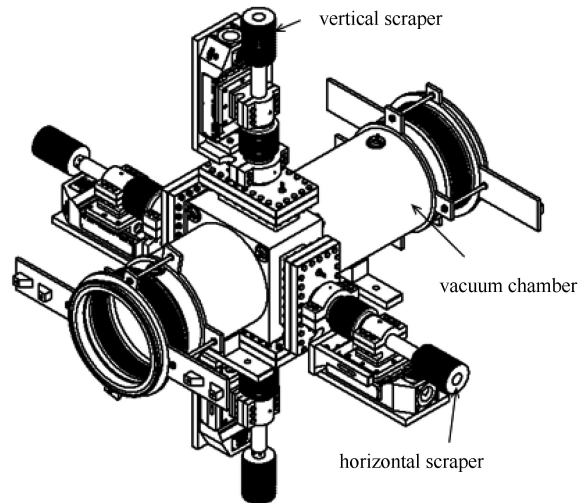


Fig. 1. Schematic view of the primary collimator.

Three kinds of metal, copper, tungsten and tanta-

Received 10 July 2012

1) E-mail: zouyq@ihep.ac.cn

©2013 Chinese Physical Society and the Institute of High Energy Physics of the Chinese Academy of Sciences and the Institute of Modern Physics of the Chinese Academy of Sciences and IOP Publishing Ltd

lum, have been considered as material of the primary collimator for their high melting point and good thermal conductivity. The thicknesses of the materials are optimized for providing efficient scattering angles and high collimation efficiency. The parameters of different materials are listed in Table 1.

Table 1. Three materials scraper energy and power loss.

materials thickness/mm	energy loss $\Delta E/\text{MeV}$	power deposition/N(W)	Max power density/(W/m <sup>2</sup> )
Ta(0.2 mm)	1.23	102.3	7.915e6
W(0.17 mm)	1.24	103.2	7.985e6
Cu(1.0 mm)	4.38	364.4	28.21e6

In order to provide an adequate scattering angle, the scrapers need to be very thin ( $<1$  mm), which results in high energy deposition. Excessive temperature rise or inhomogeneous temperature distribution induced thermal stress effects may cause serious damage to the collimator. So the thermal analysis and properly designed cooling structure are necessary for the reliability of the collimator.

In this article, we first present the energy deposition caused by beam loss on the primary collimator. The expected time structure of the beam is taken into account. Then thermal and mechanical analyses for different materials are performed by using ANSYS code. Steady state heat transfer analysis is performed to determine the temperature distribution. Based on the analysis, the cooling structure is designed and optimized with chin numbers and wind velocity. Finally, the fatigue lifetime under thermal shock is estimated with transient thermal analysis.

## 2 Energy deposition calculation

The average power deposition on the primary collimator can be estimated by the following formula

$$\bar{P}(W) = nef\Delta E, \quad (1)$$

where  $n$  is the number of particles hitting the primary collimator,  $e$  is the charge of an electron,  $f$  is the repetition rate of the RCS, and  $\Delta E$  is the ionization energy loss of the particle during interaction with the collimator.

Assuming 10% of the total beam will interact with the primary collimator. The ionization energy loss and the average beam power deposition of different materials in the collimator are shown in Table 1.

The beam loss distribution on the primary collimator is estimated by using ORBIT code [5]. A realistic beam distribution obtained by painting injection is tracked and accelerated from 80 MeV to 1.6 GeV in the presence of space charge. We project the integrated beam losses in the scraper onto the transverse plane, and fit the beam loss distribution with Gaussian functions as shown in

Fig. 2. The particle loss is mainly concentrated in the range:  $-25 \text{ mm} < W < 25 \text{ mm}$ ,  $0 < H < 3 \text{ mm}$ . The corresponding average power density distribution is expressed as

$$P(W/\text{mm}^2) = \frac{N}{2p \times 8.2} \exp\left(-\frac{(x+0.7)^2}{2 \times 8.2^2}\right) \times \left(\frac{28.4}{1.8} \exp\left(-\frac{(y+3.3)^2}{2 \times 1.8^2}\right) + \frac{741.2}{0.5} \exp\left(-\frac{(y+1.9)^2}{2 \times 0.5^2}\right)\right), \quad (2)$$

where  $N$  is the average power deposition in the first three milliseconds,  $x$  and  $y$  are the transverse positions in the  $W$  and  $H$  direction in the transverse plane with unit of mm, and the origin  $x=y=0$  locates at the center of the edge close to the beam.

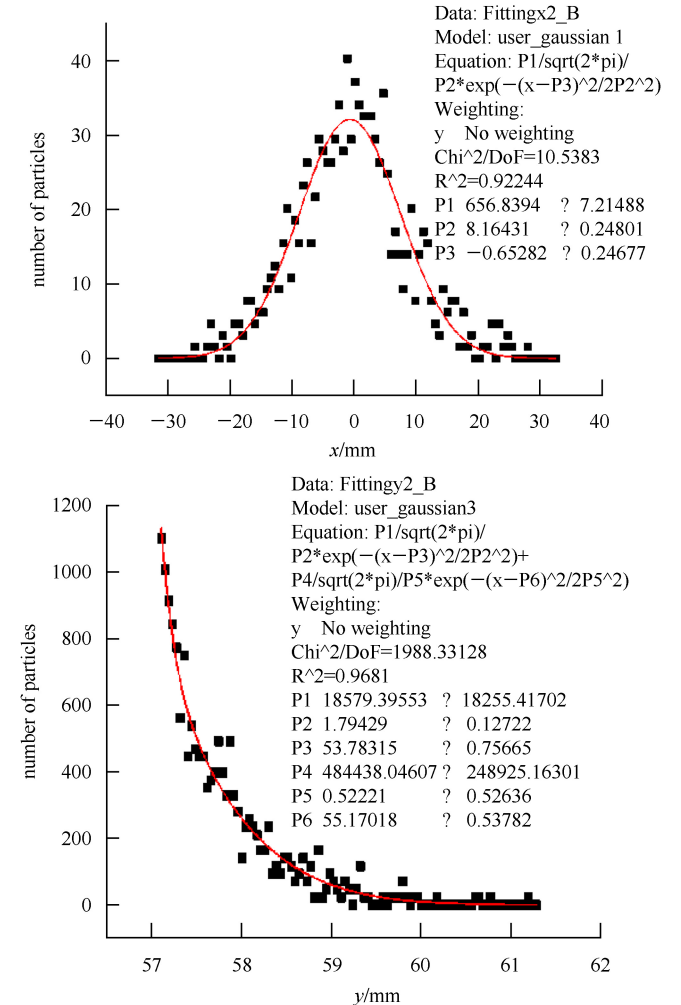


Fig. 2. Fitting of the beam loss distribution (Top: width, Bottom: height).

The time structure of the beam loss distribution is also considered. Fig. 3 shows the beam power loss distribution versus time. According to the simulations, the beam losses mostly occur during the first three milliseconds with average beam energy of 100 MeV.

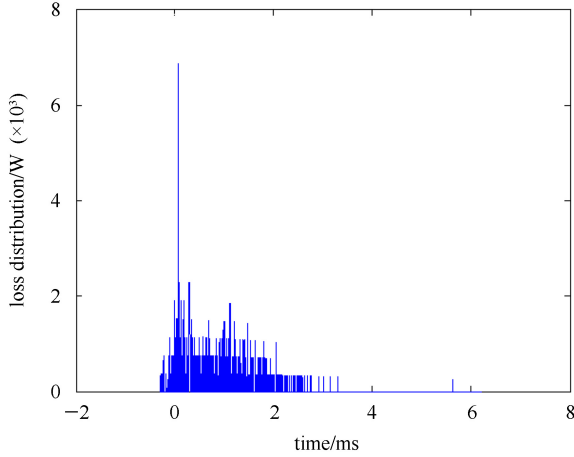


Fig. 3. The beam power density loss distribution vs. time.

### 3 Cooling structure design

Figure 1 and Fig. 4 show the scheme of the scraper structure. Four primary collimator scrapers are driven by four stepping motors individually. Each scraper connects with a copper block and cooling fin by silver brazing. The primary collimator will be set in the CSNS/RCS tunnel, and the cooling fin is at room temperature. The cooling structure consists of 15 pieces of chins with separation of 9 mm.

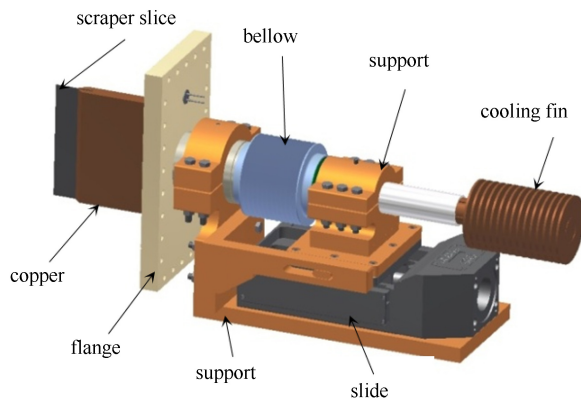


Fig. 4. The scheme of the scraper structure.

### 4 Steady-state thermal analysis

Thermal and mechanical FEM analyses are carried out with ANSYS for investigating the heat distribution and thermal stress and deformation.

#### 4.1 Heat transfer analysis

According to the characteristic of the energy deposition, steady-state heat transfer analysis is performed to determine the temperature distribution. Convective heat transfer boundary condition is used. The FEM model of one scraper is shown in Fig. 5. Free air cooling condition has been considered. The maximum temperatures of different materials are presented in Table 2. From the result we can see that copper gives the lowest temperature rise, and tantalum presents the highest, but they are all well below the melting points.

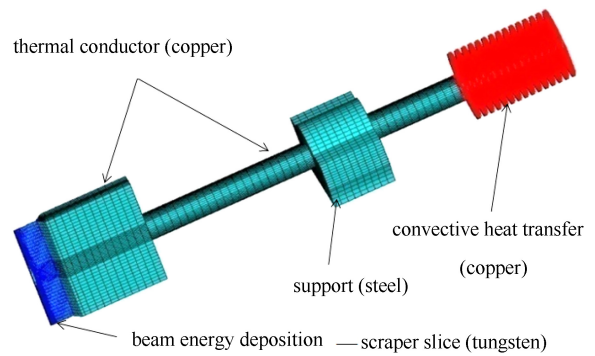


Fig. 5. The scraper FEM model and loads.

Table 2. The analysis results of different materials.

material thickness	Max temperature/K	Max Von mises stress/MPa	Max strain/mm
Ta(0.2 mm)	805.609	187	0.183
W(0.17 mm)	506.517	168	0.149
Cu(1.0 mm)	431.313	315	0.498

#### 4.2 Static stress calculation

The temperature distributions are input in structural analyses to determine the thermal stresses and displacements caused by the temperature loads. The comparison among different materials is given in Table 2. We can see that although copper presents the lowest temperature rise, the stress induced by the heat load exceeds the allowable stress of copper and the deformation is too large. Compared with tantalum, the temperature of the tungsten scraper is relatively low; the maximum stress of tungsten scraper is lower and it can get better mechanical properties; the deformation of tungsten is smaller and it can get better precision. Based on the above analysis, tungsten is chosen for the material of the CSNS/RCS primary collimator. The analysis and simulation of the following chapters are for tungsten scrapers. The temperature distribution of the tungsten scraper is shown in Fig. 6. and Fig. 7 presents the Von Mises stress distribution of the tungsten scraper.

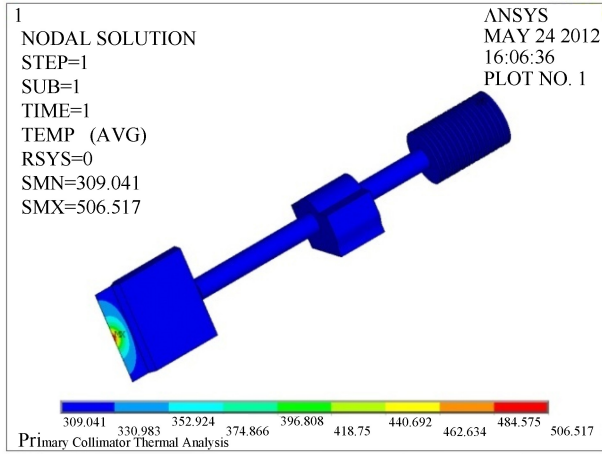


Fig. 6. The temperature distributions of the tungsten scraper.

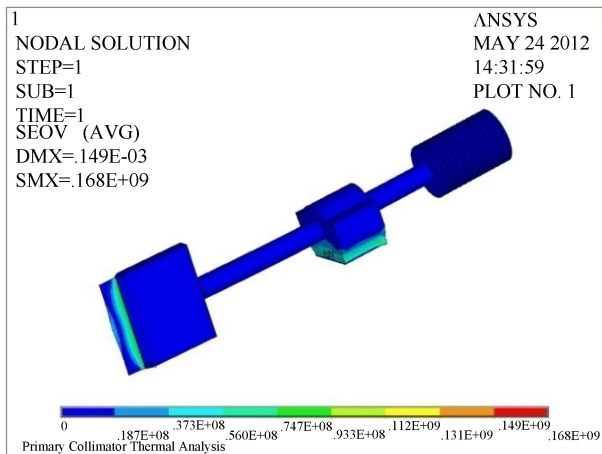


Fig. 7. The Von Mises stress distributions of the tungsten scraper.

The regions of the interface of different materials, the centralized heat source and the fixed constraint support are the dangerous areas. These should be carefully designed and taken into serious consideration in the process of manufacture.

## 5 Cooling efficiency

### 5.1 Cooling efficiency of different chin numbers

There are a number of studies on the air-cooling of air-cooled engine fins. The average fin surface heat transfer coefficient can be obtained using the following equation [6]

$$\alpha_{\text{avg}} = \left( 2.47 - \frac{2.55}{p^{0.4}} \right) \mu^{0.9} + 0.0872p + 4.31, \quad (3)$$

where  $p$  is the fin pitch, and  $\mu$  is the wind velocity. The equation is valid when  $\mu$  is in the range of 0 to 60 km/h.

Assuming free air-cooling condition, we can get the maximum temperature of scrapers with different fin numbers. The results are shown in Fig. 8.

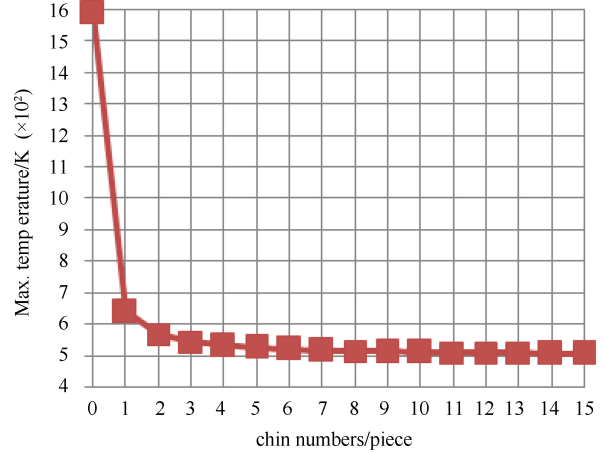


Fig. 8. Max temperature vs. chin numbers.

As shown in the plot, the temperature drops dramatically due to the introduction of cooling fins. With the increasing of the chin numbers, the temperature saturates when the number of chin is larger than 5. The results further prove that an air cooling structure is necessary for controlling the temperature rise induced by the heat load. We can design or purchase optimum air-cooled fins according to the results.

### 5.2 Cooling efficiency of different wind velocity

Generally, forced air cooling can greatly improve the air cooling effect. But this is not the case in the thermal analysis of the primary collimator in the RCS. The

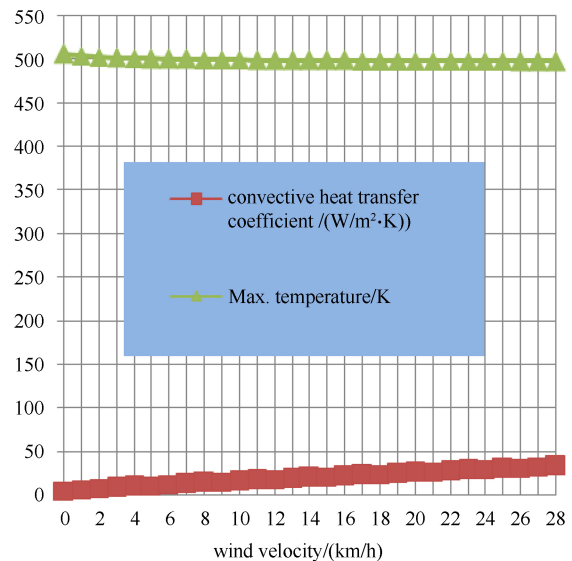


Fig. 9. Max temperature, heat transfer coefficient vs. wind velocity.

temperature changed very little by increasing wind velocity in our estimation. The relation of the maximum temperature and convective heat transfer coefficient with the wind velocity is shown in Fig. 9. So the forced air cooling system is not necessary in the CSNS/RCS primary collimator cooling structure.

## 6 Transient thermal analysis

In order to simplify the calculation, an equivalent beam power deposition in the first three milliseconds is assumed in the transient thermal analysis. The temperature approximately reaches a steady state around 60000 s (about  $1.5E6$  cycles). The result is shown in Fig. 10. The temperature vibrates between 487 K and 521 K in one period, which corresponds to a maximum temperature difference of 34 K.

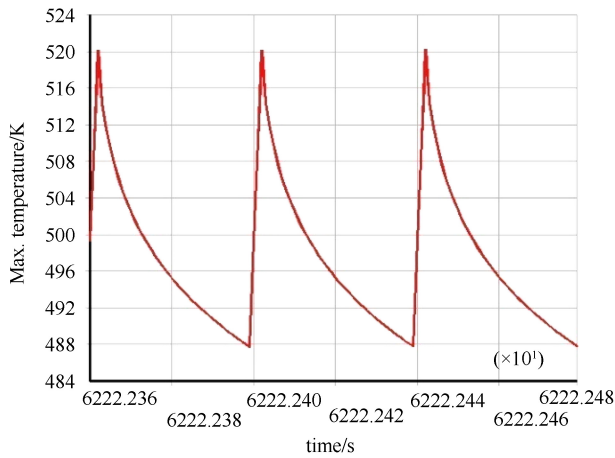


Fig. 10. The scraper static-state temperature versus time.

Based on the transient thermal analysis, the thermal shock stress is estimated. Fig. 11 shows the results of maximum period stress vs. time in the first 10 periods.

The maximum Von Mises stress temperature difference within one period is about 37 MPa. The fatigue

limit stress can be expressed by

$$\sigma_0 = 1.6Hv \pm 0.1Hv \quad [7], \quad (4)$$

where  $Hv$  is the Vickers hardness in  $\text{kgf/mm}^{-2}$ .

The Vickers hardness of tungsten in 506 K is about  $100 \text{ kgf/mm}^{-2}$  [8]. The fatigue limit stress is about 160 MPa which is much larger than the maximum period stress. So the scrapers are not supposed to suffer a fatigue failure by thermal shock.

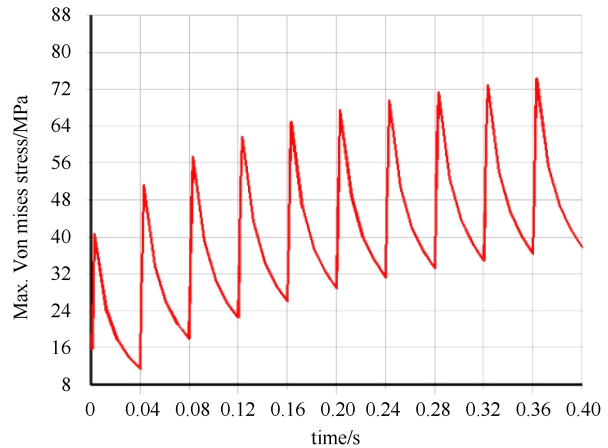


Fig. 11. The scraper maximum Von Mises stress versus time.

## 7 Conclusions

Through the above analysis and simulation, we can draw the following conclusions. (1) From the simulation of the thermo-mechanical properties of three different materials, tungsten is finally chosen as the material of the CSNS/RCS primary collimator for its lower temperature rise and better mechanical performance. (2) The air-cooled fin is necessary and the forced air cooling system is not needed in the CSNS/RCS primary collimator cooling structure. (3) The scraper will not suffer a fatigue failure by thermal shock from the transient thermo-mechanical analysis.

## References

- 1 WANG Sheng, FANG Shou-Xian, FU Shi-Nian et al. Chinese Physics C (HEP & NP), 2009, **33**(S2): 1–3
- 2 WEI Tao, QIN Qing. Nucl. Instrum. Methods Phys. Res. A, 2006, **566**(2): 212–217
- 3 WANG Na, WANG Sheng, HUANG N et al. Proc. of HB2010. Morschach, Switzerland, 2010. 572–575
- 4 Jeanneret J B. Phys. Rev. ST Accel. Beams, 1998, **1**: 081001
- 5 Galambos J et al. ORBIT User's Manual, SNS/ORNL/AP Technical Note 011. 1999
- 6 Masao YOSHIDA, Soichi ISHIHARA, Yoshio MURAKAMI et al. JSME International Journal, Series B, 2005, **71**(709): 2324–2330
- 7 Bennett J R J, Skoro G P, Booth C et al. Journal of Nuclear Materials, 2008, **377**(1): 285–289
- 8 Pisarenko G S, Borisenko V O et al. Ukrainian Periodical, Dopovidi Akademii Nauk Ukrain's'koi PSR, 1962, **8**: 1053–1056